

## RESEARCH PAPER

## MICROSTRUCTURE AND TENSILE PROPERTIES OF A RECENT INTER-CRITICALLY AUSTENITIZED QUENCHED AND PARTITIONED STEEL

*Hoda Refaiy<sup>1</sup>, Hoda Nasr El-Din<sup>1</sup>, Mai Mohamed Kamal Fouad<sup>2</sup>, Eman El-Shenawy<sup>1</sup>*<sup>1</sup> Plastic Deformation Department, Central Metallurgical R& D Institute (CMRDI), El-Felzat St., Cairo, P.O. 11722, Egypt.<sup>2</sup> Chemical Engineering Department, Faculty of Engineering, Cairo University, Cairo University St., Cairo, P.O. 12316, Egypt.\*Corresponding author: [eng\\_huda\\_refaiy@yahoo.com](mailto:eng_huda_refaiy@yahoo.com), tel, +2 01063432284, Central Metallurgical R& D Institute (CMRDI), P.O. 11722, Helwan, Egypt.

Received: 12.08.2022

Accepted: 25.10.2022

## ABSTRACT

Quenched and partitioned steel is a promising grade of advanced high-strength steel "Third Generation" for industrial applications such as the automotive industry. This research aimed to develop a novel ultra-high-strength quenched and partitioned steel with good ductility from a novel alloy with the composition of 0.37C- 3.65Mn- 0.65Si- 0.87Al- 1.5Ni-0.05P, wt.% which is non-standard. This quenched and partitioned steel was developed by inter-critical austenitization followed by quenching to a temperature below Martensite start temperature (80 and 120 °C), then partitioning at 450 °C for different times (20, 40, 60, 100, 140, and 180 s). Scanning electron microscope and X-Ray diffraction were utilized to investigate the microstructure and retained austenite characteristics. The tensile properties of developed Q&P specimens were also investigated. The results demonstrated that the specimen quenched at 120 °C and partitioned for 180s achieved a maximum strength elongation balance of 26 GPa %. Both the specimens quenched at 80 and 120 °C displayed a decrease in strength values with extending holding time due to the tempering of primary martensite. Increasing partitioning time for the specimens quenched at 120°C led to enhancing elongation, where a maximum total elongation of 19.7% was achieved for the partitioning time of 180s.

**Keywords:** Advanced High Strength Steel; Quenching and Partitioning; Martensite tempering; Retained Austenite; Tensile Properties

## INTRODUCTION

Advanced high strength steels (AHSSs) have attracted significant attention for automotive applications in the last years. This is because they have superb mechanical properties that promote producing lighter vehicle parts and contribute to solving environmental and energy issues. AHSS steel displays better strength and ductility than high-strength steel (HSS) [1].

Quenched and partitioned (Q&P) steel is a recent grade of third-generation advanced high-strength steel which has been first developed by J. Speer [2]. Q&P steel is characterized by its exceptional tensile properties over other AHSS types[3]. The outstanding mechanical properties of Q&P steels are a result of their structure which consists of ferrite, martensite lathes, and retained austenite [4]. The martensite phase in the Q&P steel microstructure enhances the yield strength while ductility and work hardening are improved due to the transformation-induced plasticity (TRIP) effect of retained austenite [5]. The gradual mutation of stabilized austenite in quenched and partitioned steel postpones occurrence of necking during straining and consequently improves the ductility [6]. Additionally, C. Zhou et al reported that existence of retained austenite in ultra- high strength steel structure enhances cryogenic toughness [7].

In order to acquire a Q&P steel microstructure, it is essential to choose the convenient composition and processing conditions that attains the stabilization of retained austenite during pro-

cessing, restrain carbide precipitation, and formation of secondary [8–11]. Alloying elements of Silicon, Aluminum, and Manganese are added to Q&P steel to slow carbide precipitation and enhance the retention of a high proportion of retained austenite in the final microstructure [2,12]. Moreover, some elements such as Carbon, Manganese, Silicon, Molybdenum, and Copper increase the yield strength of ferrite in steel [13].

The two-step heat treatment process for Q&P steel consists of quenching the prior austenite phase or austenite-ferrite mixture to a quenching temperature (QT) below martensite start ( $M_s$ ) and above martensite finish ( $M_f$ ) temperatures, followed by partitioning at the same quench temperature or higher, and finally quenching to room temperature [14,15]. The carbon content in martensite decreases during the partitioning process, and it diffuses from martensite into primary austenite, which did not transfer during the first quench. Consequently, the  $M_s$  temperature decreases to be below room temperature and untransformed austenite becomes more stable [16,17].

The mechanism of carbon diffusion from martensite to austenite is still under research and debate among scientists [9,18,19]. J. Speer et al. reported that carbon diffusion from martensite to untransformed austenite is controlled by the constrained carbon equilibrium criterion (CCE) [10]. Another study indicated that this stage follows two suggested pathways where the carbon is first dispersed into untransformed austenite from supersaturated martensite; thereafter, the carbon enrichment of austenite is aided by the produced carbide-free bainite [15].

This research aims to develop ultra-high strength quenched and partitioned steel from the alloy with a chemical composition of 0.37C-3.65Mn- 0.65Si- 0.87Al- 1.5Ni- 0.05P, (wt.%) and heat treating by inter-critical austenitization then applying a two-step quenching and partitioning process. The innovation of this study is to develop quenched and partitioned steel from a novel chemical composition which is nonstandard and depended on reducing the percentage of silicon and adding other alloying elements. Hence, it is important to determine the proper heat treatment conditions for the recent alloy in order to achieve optimal mechanical properties and galvanize-ability. The appointed objectives are investigating the impact of processing conditions encompassing quench temperature (QT) and partitioning time (Pt) on morphological changes, retained austenite characteristics, and tensile properties.

**MATERIAL AND METHODS**

Developing ultra-high-strength steel with excellent ductility by quenching and partitioning process depends firstly on determining the proper alloy chemical composition and choosing the convenient heat treatment conditions. **Table 1** displays the percentages of the alloying elements in the studied alloy, including Mn, Si, Al, P, and Ni. An induction furnace was used for producing the alloy from steel scrap, and ferroalloys of (Fe-80% Mn), and Si (Fe-75%Si) while Ni and Al were added as pure metals.

The as-cast alloys were machined to sections with dimensions of 200mm×60mm×40mm, then homogenized at 1250°C for 2hrs, followed by furnace cooling. The dilatation test was implemented before the heat treatment process to allocate the actual transformation temperatures by using Gleeble 3500 machine, so some homogenized sections of the alloy were hot forged into bars then the specimens for this test were prepared according to Gleeble's standard. The dilatation curve of the alloy is shown in **Figure 1** where transformation temperatures of AC<sub>1</sub>, AC<sub>3</sub>, and Ms are determined to be 720, 810, and 260 °C, respectively [10]. The other homogenized sections were hot forged to plates with a thickness of 7mm, then hot-rolled at 1100 °C to sheets with 1.8mm thickness through four passes. Then, the developed steel sheets were machined before the heat treatment process into small specimens (for microstructure and XRD investigations) and tensile specimens, which followed the ASTM E8 standard with a total parallel length of 32mm and a width of 6mm.

**Table 1** Chemical composition of the investigated alloy, (mass, %)

C	Mn	Si	Al	Ni	P	S	Fe
0.37	3.65	0.65	0.87	1.5	0.05	0.015	Balance

**Figure 2** indicates the implemented quenching and partitioning heat treatment cycles of the specimens. These cycles are composed of inter-critical austenitization at 780 °C for 10 min, then quenching at two different temperatures of 80 and 120 °C, where about 84 and 75% of prior austenite (which forms above AC<sub>1</sub>), respectively, are expected to transform into primary martensite during the first quench. These percentages are calculated by the K-M relationship (Eq. 1)[14]. The quenching stage is followed by partitioning at 450°C for different holding times (Pt) (from 20 to 180s).

$$f_M = 1 - e^{-0.011 \cdot (M_s - T_q)} \tag{Eq.1}$$

Where:  $f_M$ - volume fraction of primary martensite

$M_s$ - martensite starts temperature, and quench temperature.  
 $T_q$ - quench temperature

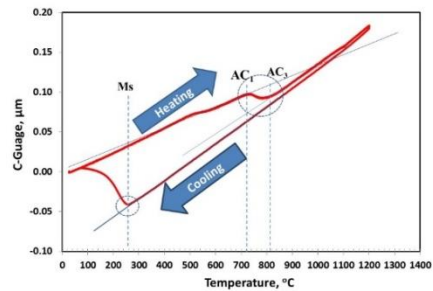


**Fig. 1** Dilatation curve of the investigated steel alloy [10].

Prior to studying the microstructure and X-Ray Diffraction (XRD) of the quenched and partitioned specimens, they were metallographically prepared by grinding on an abrasion machine, then polishing using alumina paste. The specimens were finally etched in 2% nital to investigate the microstructure by FE-SEM. Cu target X-Ray Diffraction (XRD) was utilized at 45 kV and 40 mA to measure retained austenite percentages and its carbon content in the developed Q&P specimens. The volume fraction of retained austenite ( $V_\gamma$ ) was calculated from Eq.2,

$$V_\gamma = \frac{I_\gamma k_\alpha}{I_\gamma k_\alpha + I_\alpha k_\gamma} \tag{Eq. 2}$$

Where:

$I_\gamma$  - the average integrated intensity obtained at the (200) $\gamma$ , (220) $\gamma$ , (311) $\gamma$ , and (200) $\alpha$ , (211) $\alpha$  diffraction peaks

$I_\alpha$  - the average integrated intensity obtained at (200) $\alpha$ , (211) $\alpha$  diffraction peaks

$K_\gamma$  are the reflection coefficients of austenite phase

$K_\alpha$  - the reflection coefficients of ferrite phase

The average carbon contents in retained austenite for the specimens are calculated from equation 3 [14,20,21].

$$a = 3.556 + 0.0453xC + 0.00095xMn + 0.0056xAl + 0.0006xCr \tag{Eq. 3}$$

Where:  $(\bar{A})$ - average lattice constant of (200) $\gamma$ , (220) $\gamma$ , (311) $\gamma$  diffraction peaks  $x_C$ ,  $x_{Mn}$ ,  $x_{Al}$  and  $x_{Cr}$ - weight percentages of C, Mn, Al, and Cr, respectively.

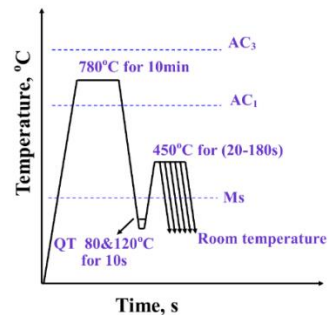


**Fig. 2** Heat treatment cycles for the investigated alloy.

The tensile properties of heat-treated specimens were measured at room temperature using the uniaxial tensile test (LFM-L 20 KN) at 1 mm/min crosshead speed.

## RESULTS AND DISCUSSION

### Microstructure of studied Q&P specimens

The scanning electron micrographs of the specimens heat-treated by inter-critical austenitization at 780°C, then quenching at 80 and 120 °C and partitioning at 450 °C for 20, 100, and 180s are shown in **Figures 3 (a-f)**. It can be observed that both ferrite, tempered primary martensite (M<sub>1</sub>), a small percent of retained austenite (RA), and other secondary phases, which include bainite (B), blocky martensite (M<sub>2</sub>) are existed in the microstructure of all specimens. The deficient partitioning of carbon during the partitioning stage from formed primary martensite to unconverted austenite is involved in the formation of secondary phases. Moreover, the microstructure of the specimens quenched at 120 °C for 100s and 180s is finer than the microstructure of quench temperature 80 °C, which is partitioned for the same time.

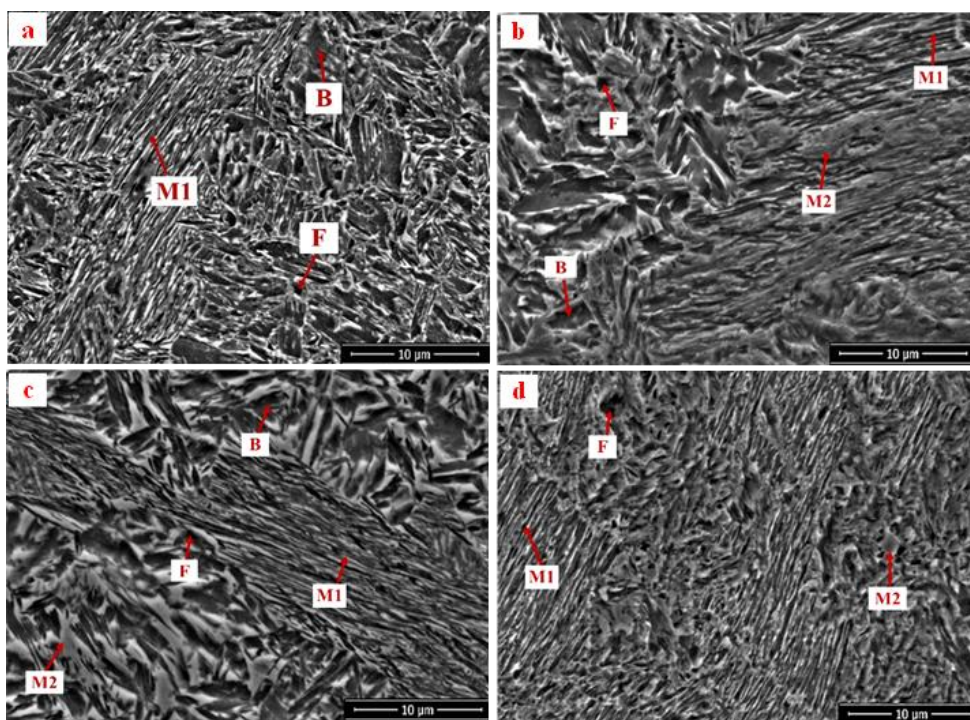
### Retained austenite volume fraction and its carbon content of studied Q&P specimens

**Figures 4a** and **Figures 4b** demonstrate the peak intensity of phases for developed Q&P steel specimens, quenched at 80 and 120 °C then partitioned for different times (from 20 up to

180s). The XRD patterns confirm that the FCC structure phase is present.

**Tables 2** and **3** demonstrate calculated retained austenite volume percentages and their carbon content of heat-treated specimens. It is noticeable that the percentages of the retained austenite fractions are relatively low and do not exceed 4% for both quench temperatures. The low quench temperature of 80 °C achieved the highest retained austenite value of 4% for partitioning time of 100s, while the retained austenite values for other partitioning times (20, 40, 60, 140, 180) ranged between 1.1 and 2%. On the other hand, the short partitioning time of 20s at a quenching temperature of 80 °C resulted in the formation of maximum retained austenite percentage (4%), while a further increase in holding time at partitioning temperature above 20s slightly affected the fraction of stabilized austenite where these values are between 2 and 2.7%.

The values of carbon content in retained austenite for the specimens quenched at 80 °C for different partitioning times are lower than the values for quench temperature 120 °C, which partitioned for the same time except for the partitioning time of the 60s and 180s. The specimen quenched at 80 °C and 120 °C then partitioned for the 60s achieved a maximum carbon content about 1.12%. The carbon content values for the specimens quenched at 80 °C then partitioned for different times are very close or nearly the same of 120 °C values except at partitioning time 20s.



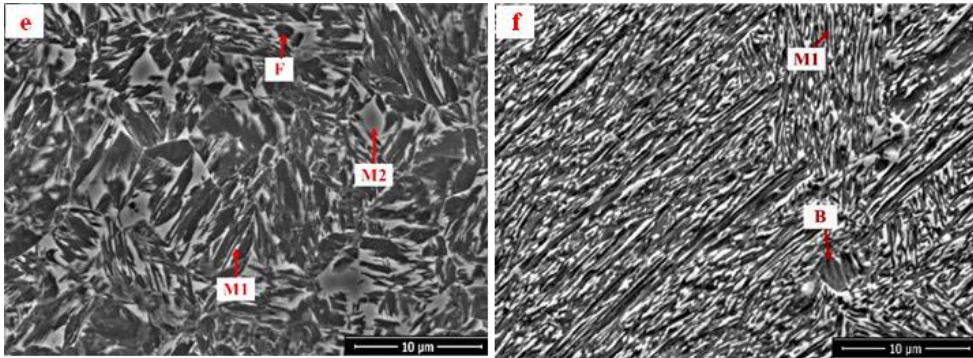


**Fig. 3** Scanning electron micrographs of specimens quenched at 80°C (a, c, and e) and 120 °C (b, d, and f), then partitioned at 450 °C for (a and b) 20s, (c and d)100s, and (e and f-180s).

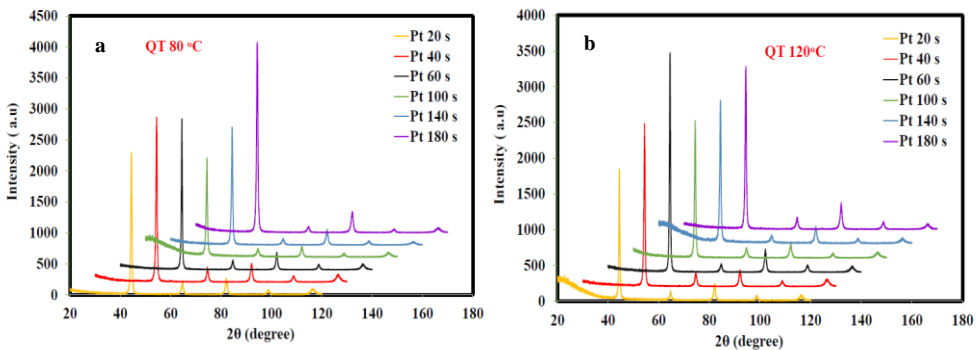


**Fig. 4** XRD diffraction peaks of specimens quenched at (a)80 °C and (b) 120 °C then partitioned at 450 °C for different times (20s up to 180s).

**Table 2** Volume fraction of retained austenite, % for developed Q&P steel.

Pt (s)	20	40	60	100	140	180
QT 80°C	1.1	1.3	2	4	1.3	1.6
QT 120°C	4	2.4	2.1	2.7	2.5	2

**Table 3** Carbon content in retained austenite, % for developed Q&P steel.

Pt (s)	20	40	60	100	140	180
QT 80°C	0.62	0.9	1.13	0.93	0.8	0.9
QT 120°C	0.9	0.9	1.12	1.04	0.97	0.89

It is evident from **Tables (2-3)** that applied conditions of quenching and partitioning regimes resulted in low values of retained austenite with lower carbon content, especially at quench temperature 80 °C. This may be due to the occurrence of side reactions that resulted in the formation of bainite, martensite, and precipitation of carbides (see Figures 3 a-f). This interpretation is matched with the finding of some previous studies [9,16,17,22], which showed that partitioning of carbon is not completed due to segregation or clustering or enhancement of carbide formation. The carbide precipitation consumes the available carbon in the martensite, which diffuses to untransformed austenite during partitioning [9,16,17,22,23]. Podder et al. [24] reported that the tempering stage of the bainitic steel which composed of bainitic ferrite,

martensite, and retained austenite firstly resulted in martensite tempering and cementite precipitation from supersaturated austenite. This stage leads to decreasing retained austenite percentage at room temperature. After the previous transformation during tempering, the austenite is transformed into ferrite and another amount of carbides [24]. As previously mentioned, the side reactions during partitioning, which result in carbide formation, usually are not averted despite the existence of high Si and Mn content in the composition of the alloy [25]. The slight rise in the volume of retained austenite and carbon content of specimens quenched at 120 °C compared to specimens quenched at 80°C may be attributed to the formation of a higher amount of bainite at this temperature which involves with primary martensite in stabilizing austenite. This is congruent with the results of preceding research which demonstrated that formation of bainite during partitioning for high quench temperatures participated with martensite to enrich carbon in austenite and increased its retention [26].

**Tensile properties of studied Q&P steel specimens**

**Figures 5a** and **5b** demonstrate engineering stress-strain curves of heat-treated specimens. All the specimens exhibited a continuous yielding behavior. This may be attributed to the presence of some nitride-forming elements, such as Al and Si, which decrease carbon and nitrogen interstitial atoms that impede dislocation movement [27]. Consequently, the mobile dislocation density is increased [28].

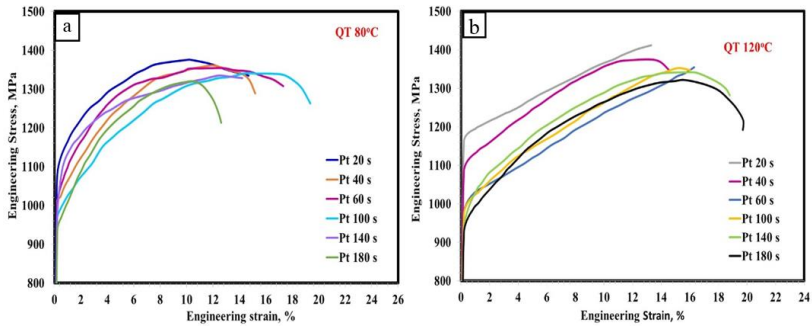


**Fig.5** Engineering stress-strain curves of Q&P steel specimens quenched at (a) 80°C, and (b)120°C, then partitioned at 450°C for different times (from 20s up to 180s).

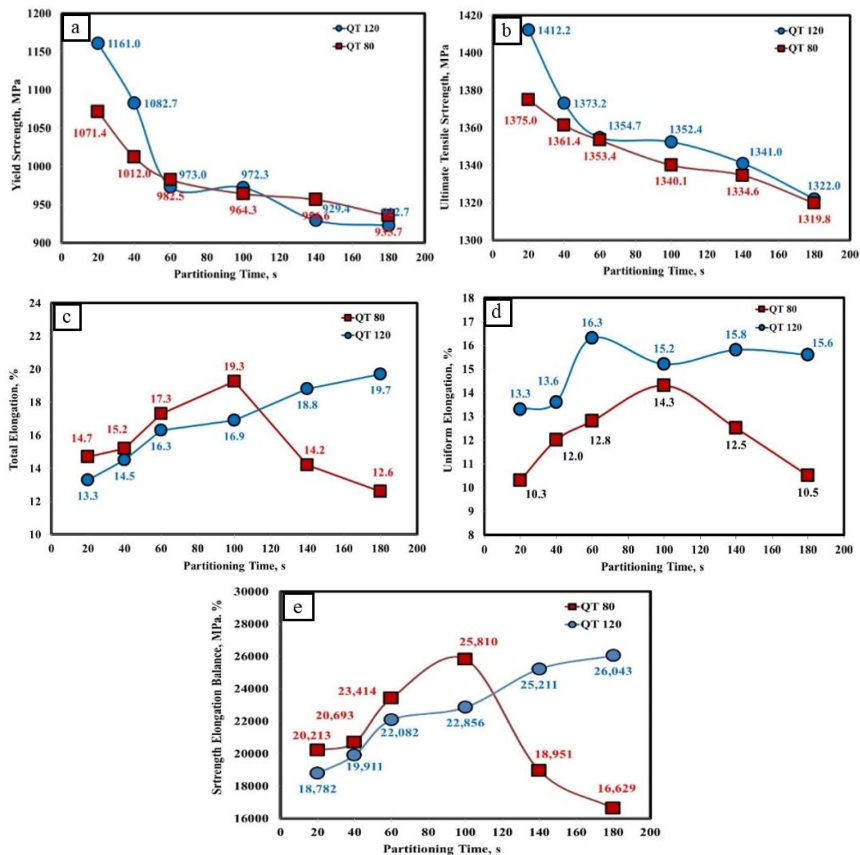


**Fig. 6** Variation of a- ultimate tensile strength and b- total elongation with partitioning time for developed Q&P steel quenched at 80 and 120 °C.

**Figures 6 (a-e)** show the change of yield and ultimate tensile strength, total and uniform elongation, and strength elongation balance with partitioning time for developed Q&P steel quenched at 80 and 120 °C. The yield and ultimate tensile strength showed the same behaviour where they declined with increasing partitioning time. The YS of the samples quenched

at 120°C sharply declined from 1161 to 973 MPa with increasing partitioning time from the 20s to 60s; then, it gradually diminished to 922.7MPa with excess partitioning to 180s. In comparison, quenching at 120 °C then partitioning for different times (20s to 180s) resulted in a gradual decline of YS from 1071.4 to 933.7MPa.

The ultimate tensile strength (UTS) of specimens quenched at 120°C is slightly larger than these values of specimens quenched at 80 °C and partitioned for the same time except at partitioning time 20s where the specimen quenched at 120°C for 20s achieved a higher UTS more than QT 80 °C partitioned for the same time by about 40 MPa (Figure 6 b). For QT 120 and 80°C, the UTS went down from 1412 to 1322MPa and from 1375 to 1319.8 MPa, respectively, with an increasing holding time from the 20s to 180s. However, increasing Pt from 60s to 100s at QT 120 °C slightly affected UTS. The total elongation (TEL) of specimens quenched at 80°C firstly increased with increasing time until 100s to a maximum value of 19.3%, then it decreased to 12.6% with further increase in Pt to 180s, but the TEL of specimens quenched at 120 °C gradually increased to a value of 19.7% with further increase in Pt to 180s (Figure 6 c). Moreover, the uniform elongation (UEL) of specimens quenched at 120°C demonstrated higher values than quench temperature 80 °C at all partitioning times as well as the values of UEL for specimens quenched at 80 °C are lower than values of their total elongation (Figure 6 d). The UEL for two quench temperatures (80

and 120 °C) increased with increased partitioning time; then it decreased where the UEL for QT 120 °C went up to a peak value of 16.3% until Pt 60s, then it slightly decreased with further increase in holding time.

As clearly in Figure 6 e, the strength elongation balance (SEB) for QT 80 and 120 °C also shows a similar trend to TEL. For QT 80 °C, it ascended to the peak value of 25.8GPa. % with increasing holding time to 60s, then gradually decreased to a lower value of 16.6 GPa.% at prolonged Pt of 180s. The SEB of specimens quenched at 120°C is gradually increased to the maximum value of 26 GPa.% with increase in holding time during partitioning to Pt 180s.

Figures 7&8 demonstrate the relation between logarithm true stress and logarithm true strain for the developed Q&P specimens, which were quenched at 80 and 120 °C and partitioned for different times (20 -180s). The fitting line represents the strain hardening exponent (n). It is obvious that all the specimens have two n-values and the strain at which the n-value changes is called a critical strain, where martensitic transformation starts at this point.

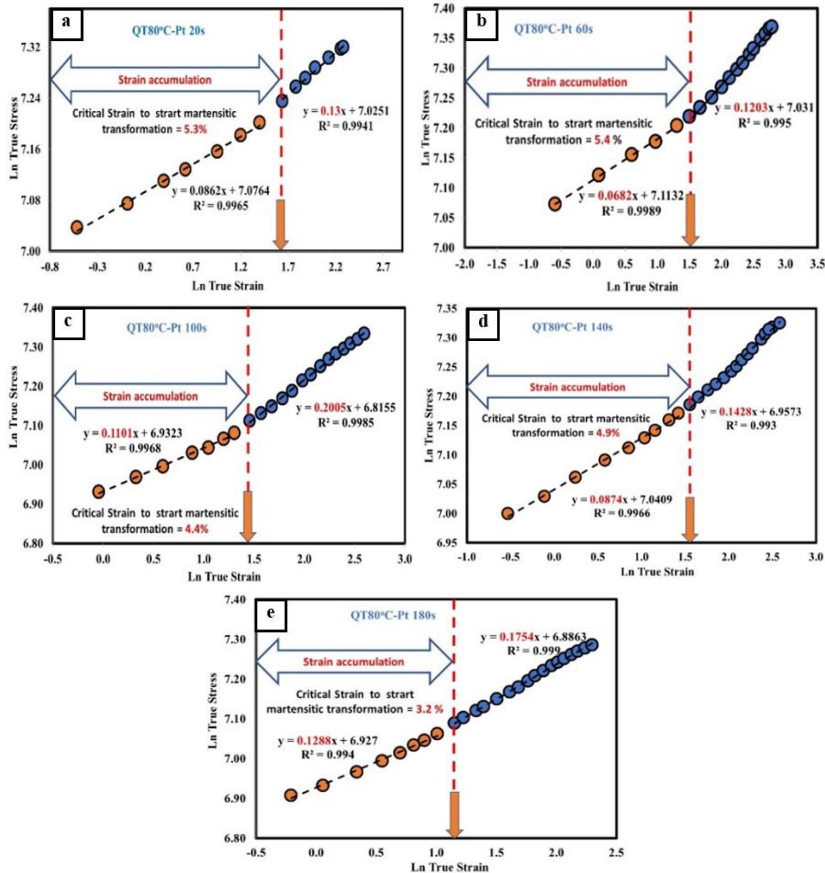


Fig.7. Variation of true stress with true strain for Q&P specimens quenched at 80 °C then partitioned for a-20s, b-60s, c-100s, d-140s, e- 180s.

Tables 4 and 5 comprise the n-values and the critical strain for developed Q&P specimens heat-treated at different conditions.

As shown in Table 4, the specimens quenched at 80 °C and partitioned at times from 20s up to 140s resulted in high n1

values, which ranged between 0.07 and 0.11, while Pt 180s exhibited the maximum n1 value of 0.13. The n2 value for the same specimens gradually increased with increasing holding time to the peak value of 0.2 for Pt 100s; then, it decreased with further augmentation in holding time. Whereas the short partitioning time of 20s and 60s resulted in high critical strain above 5%, then it gradually went down with an additional increase in partitioning time where it achieved the lowest value of 3.2% after the longest holding time of 180s.

It is noticed from **Table 5** that the n1 value of specimens quenched at 120 °C and partitioned for a time more than 60s is slightly affected by increasing partitioning time, where it is about 0.1, while the short partitioning time of 20s resulted in a lower n1 value of 0.06. At the same time, the n2 value for all specimens quenched at 120°C is considerably higher than any other quenched and partitioned specimens (equal to 0.2 or above). This value is enhanced from 0.2 to a peak value of 0.28 with increasing holding time from the 20s to 60s, then it diminished to reach 0.2 again with further increase in partitioning time to 180s.

Although the developed quenched and partitioned specimens attained relatively lower percentages of retained austenite, they exhibited good tensile properties. This assures that not only the retained austenite volume fraction and its carbon content are the main affecting factor on the tensile properties of the developed quenched and partitioned specimens. But, the

formed structure and size of phases also play a critical role in the tensile properties. The decrease of yield and ultimate tensile strength with increasing partitioning times for the specimens quenched at 80 and 120 °C is a consequence of primary martensite tempering after the partitioning step [10]. As previously reported, extending tempering time results in declining strength of steel due to reducing the carbon content in martensite and its solid solution strengthening [29]. For specimens quenched at 80 °C, the formation of the small amount of retained austenite (less than 2%) with lower carbon content (less than 0.9%) for short partitioning time (20s and 40s) and prolonged time (140s and 180s) have an effect on the regressive of TEL and SEB for these conditions compared to long partitioning time of 60s and 100s which has a relatively higher percentage of retained austenite and its carbon content (See **Tables 2 and 3**). Furthermore, the incomplete tempering of martensite for a short partitioning time and the formation of a higher amount of blocky and islands secondary martensite, as well as increasing its size at extended partitioning time (above 100s), are involved in decreasing TEL and SEB for these specimens. These factors, which affected the TEL at short Pt (20s and 40s) and prolonged Pt (140s and 180s), consequently affected the n2 value, which has a lower value (equal to or less than 0.17) than the n2 value for partitioning time 100s (equal 0.2), i.e., decreasing material capacity to be work-hardened.

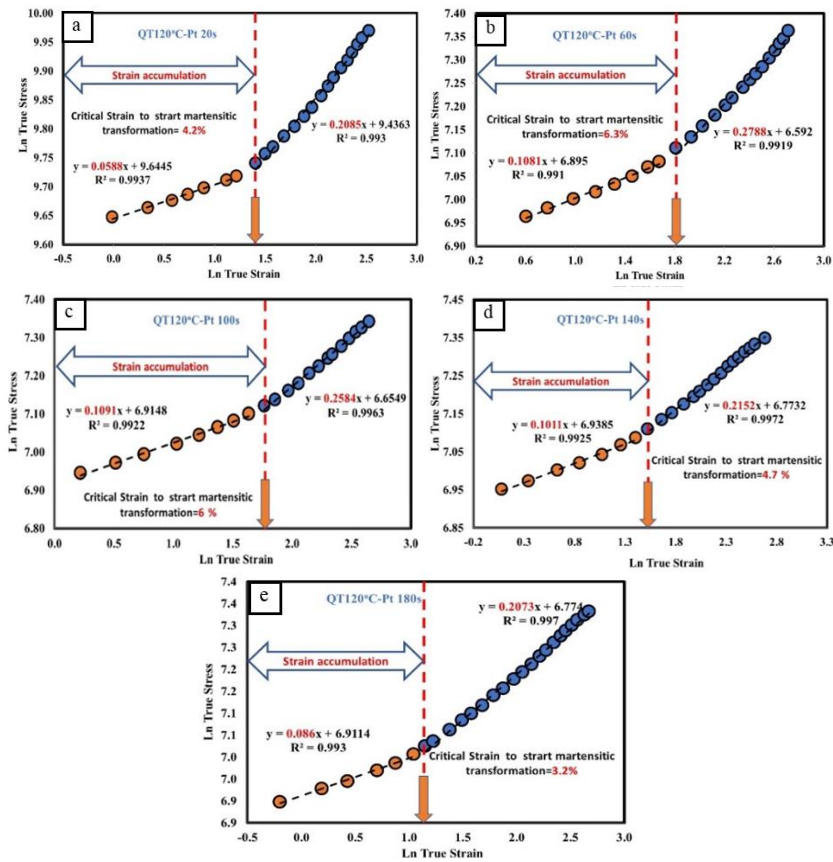


**Fig. 8.** Variation of true stress with true strain for Q&P specimens quenched at 120 °C then partitioned for a-20s, b-60s, c-100s, d-140s, e- 180s.

The specimens quenched at 120 °C displayed gradual growth in total elongation and strength elongation balance with increasing partitioning time. This is attributed to the morphologic changes rather than the retained austenite volume fraction and carbon content.

As shown in Figure 3 b, the partitioning step for a short time resulted in the formation of higher amounts of blocky and islands of secondary martensite, which deteriorate the ductility of steel. With increasing partitioning time for these specimens, the chance for more bainitic transformations to occur during the partitioning stage is promoted; therefore, the amount of untransformed austenite is consumed, and the possibility of forming more secondary martensite, which deteriorates tensile properties, is decreased. The alteration of retained austenite morphology from blocky into inter-lath films between martensite lathes at long partitioning time (180s) (Figure 3 f) also assisted in improving TEL and SEL balance.

Although the TEL and SEB have augmented with increasing partitioning time, the n2 value has relatively declined for the specimens which partitioned for a time longer than 100s. This may be due to the decline of retained austenite volume fraction, carbon content, and martensite lath's increasing length and thickness. Additionally, the high increase of n2 value for all specimens quenched at 120 °C and partitioned for different times compared to specimens quenched at 80 °C is attributed to the refinement of martensite lath thickness which consequently enhances the tensile properties.

**Table 4** values of n1, n2, and critical strain of specimens quenched at 80 °C then partitioned at 450 °C for different times.

Partitioning time (s)	20	60	100	140	180
n1	0.09	0.07	0.11	0.09	0.13
n2	0.13	0.12	0.20	0.14	0.17
Critical Strain (%)	5.3	5.4	4.4	4.9	3.2

**Table 5** values of n1, n2 and critical strain of specimens quenched at 120 °C then partitioned at 450 °C for different times.

Partitioning time (s)	20	60	100	140	180
n1	0.06	0.1	0.1	0.1	0.09
n2	0.2	0.28	0.26	0.22	0.2
Critical Strain (%)	4.2	6.3	6	4.7	3.2

## CONCLUSIONS

This research investigated developing ultra-high-strength sheet steel with good ductility via inter-critical austenitization then executing different quenching and partitioning regimes. The composition of this studied alloy included different alloying elements of 0.37C- 3.65Mn- 0.65Si- 0.87Al- 1.5Ni-0.05P, wt.%. The influence of quenching and partitioning circumstances (quench temperature and partitioning time) on the microstructure, characteristics of retained austenite, and tensile properties have also been investigated, and the results can be summarized in the following points:

- Quenching for 80 or 120 °C after inter-critical austenitization then partitioning at 450°C for different times led to forming a multiphase microstructure of primary martensite matrix, ferrite, and retained austenite as well as secondary phases of blocky martensite and bainite.
- A maximum volume fraction of 4% with a carbon content of approximately 0.9 % was achieved for the specimens quenched at 120 and 80 °C and partitioned for 20s and 100s, respectively. Additionally, quenching at 120°C resulted in a relatively higher volume fraction of retained

austenite and carbon content than quench temperature 80°C, which was partitioned for the same time.

- The yield and ultimate tensile strength of the specimens quenched at 80 and 120 °C showed a downward trend with increasing partitioning time above 60s, resulting from primary martensite tempering.
- The specimens quenched at 80 °C and partitioned for times up to 100s demonstrated better elongation and strength elongation balance than specimens quenched at 120 °C and partitioned for the same time, but the further increase in partitioning time above 100s at quench temperature 120 °C resulted in preferable values than 80 °C.
- Partitioning for longer times (140s and 180s) after quenching at 120 °C led to increasing n2 value, elongation, and strength elongation balance compared to the specimens quenched at 80°C due to the grain refinement and morphologic change, which comprised forming inter-lath retained austenite.
- The specimens quenched at 80 and 120 °C achieved a maximum strength elongation balance of approximately 26 GPa.%. The quenched and partitioned specimens achieved a maximum elongation of 19.7% with an ultimate tensile strength of 1322MPa for the specimen, which was quenched at 120 °C and partitioned for 450 °C for a prolonged time of 180s.

## REFERENCES

1. T. Kvackaj, J. Bidulská, R. Bidulský: Materials, 14, 2021, 1–20. <https://doi.org/10.3390/ma14081988>.
2. J. Speer, D.K. Matlock, B.C. De Cooman, J.G. Schroth: Acta Materialia, 51, 2003, 2611–2622. [https://doi.org/10.1016/S1359-6454\(03\)00059-4](https://doi.org/10.1016/S1359-6454(03)00059-4).
3. E. De Moor, J.G. Speer, D.K. Matlock, J.H. Kwak, S.B. Lee: ISIJ International, 51, 2011, 137–144. <https://doi.org/10.2355/isijinternational.51.137>.
4. S.H. Sun, A.M. Zhao, R. Ding, X.G. Li: Acta Metallurgica Sinica (English Letters), 31, 2018, 216–224. <https://doi.org/10.1007/s40195-017-0667-3>.
5. C.B. Finfrock, A.J. Clarke, G.A. Thomas, K.D. Clarke: Metallurgical and Materials Transactions A: 51, 2020, 2025–2034. <https://doi.org/10.1007/s11661-020-05666-8>.
6. P. Xia, F. Vercruyse, C. Celada-Casero, P. Verleysen, R.H. Petrov, I. Sabirov, J.M. Molina-Aldareguia, A. Smith, B. Linke, R. Thiessen, D. Frometa, S. Parareda, A. Lara: Materials Science and Engineering A, 831, 2022, 142217. <https://doi.org/10.1016/j.msea.2021.142217>.
7. C. Zhou, Q. Bin Ye, J. Hu, T. Zhao, X.H. Gao, Z.D. Wang: Materials Science and Engineering A. 831, 2022, 142356. <https://doi.org/10.1016/j.msea.2021.142356>.
8. D. V. Edmonds, K. He, F.C. Rizzo, B.C. De Cooman, D.K. Matlock, J.G. Speer: Materials Science and Engineering A, 438–440, 2006, 25–34. <https://doi.org/10.1016/j.msea.2006.02.133>.
9. A.J. Clarke, J.G. Speer, M.K. Miller, R.E. Hackenberg, D. V. Edmonds, D.K. Matlock, F.C. Rizzo, K.D. Clarke, E. De Moor: Acta Materialia, 56, 2008, 16–22. <https://doi.org/10.1016/j.actamat.2007.08.051>.
10. E.H. El-Shenawy, H.N. El-Din Hedia, M.M. Kama-El-Din, H.R. Badwy: Design and optimization of processing conditions for a recent quenched and partitioned steel, in: ESAFORM 2021 - 24th International Conference on Material Forming, 2021. <https://doi.org/10.25518/esaform21.4162>.
11. K. Joonas: SAE International Journal of Materials and Manufacturing, 8, 2015, 419–424. <http://doi.org/10.4271/2015-01-0530>.
12. M.J. Santofimia, L. Zhao, J. Sietsma: Metallurgical and Materials Transactions A: 40, 2009, 46–57.

<https://doi.org/10.1007/s11661-008-9701-4>.

13. G. Krauss: *Steels - Processing, Structure, and Performance*, 4th ed., ASM International, Materials Park, Ohio, 2012.

14. B. Chen, J. Liang, T. Kang, R. Cao, C. Li, J. Liang, F. Li, Z. Zhao, D. Tang: *Metals*. 8, 2018, 579. <https://doi.org/10.3390/met8080579>.

15. H.Y. Li, X.W. Lu, X.C. Wu, Y.A. Min, X.J. Jin: *Materials Science and Engineering A*. 527, 2010, 6255–6259. <https://doi.org/10.1016/j.msea.2010.06.045>.

16. Y. Toji, G. Miyamoto, D. Raabe: *Acta Materialia*. 86, 2015, 137–147. <https://doi.org/10.1016/j.actamat.2014.11.049>.

17. Y. Toji, H. Matsuda, M. Herbig, P.P. Choi, D. Raabe: *Acta Materialia*. 65, 2014, 215–228. <https://doi.org/10.1016/j.actamat.2013.10.064>.

18. S.Y.P. Allain, G. Geandier, J.C. Hell, M. Soler, F. Danoix, M. Gouné: *Scripta Materialia*. 131, 2017, 15–18. <https://doi.org/10.1016/j.scriptamat.2016.12.026>.

19. S. Dhara, S. van Bohemen, M.J. Santofimia: *Materials Today Communications*. 33, 2022, 104567. <https://doi.org/10.1016/j.mtcomm.2022.104567>.

20. D J Dyson and B Holmes: *Journal of the Iron and Steel Institute*, 208, 1970, 469–474.

21. J. Hidalgo, K.O. Findley, M.J. Santofimia: *Materials Science and Engineering A*, 690, 2017, 337–347. <https://doi.org/10.1016/j.msea.2017.03.017>.

22. G.A. Thomas, F. Danoix, J.G. Speer, S.W. Thompson, F. Cuvilly: *ISIJ International*, 54, 2014, 2900–2906. <https://doi.org/10.2355/isijinternational.54.2900>.

23. S. Ebner, R. Schnitzer, C. Suppan, A. Stark, H. Liu, C. Hofer: *Materials Characterization*, 163, 2020, 110242. <https://doi.org/10.1016/j.matchar.2020.110242>.

24. A. Saha Podder, H.K.D.H. Bhadeshia: *Materials Science and Engineering A*. 527, 2010, 2121–2128. <https://doi.org/10.1016/j.msea.2009.11.063>.

25. F. HajyAkbar, J. Sietsma, G. Miyamoto, T. Furuhashi, M.J. Santofimia: *Acta Materialia*. 104, 2016, 72–83. <https://doi.org/10.1016/j.actamat.2015.11.032>.

26. F. Peng, Y. Xu, J. Li, X. Gu, X. Wang: *Materials and Design*. 181, 2019, 107921. <https://doi.org/10.1016/j.matdes.2019.107921>.

27. H.N. El-Din, E.A. Showaib, N. Zafarani, H. Refaiy: *International Journal of Mechanical and Materials Engineering*. 12, 2017. <https://doi.org/10.1186/s40712-017-0071-9>.

28. S. Yan, X. Liu, W.J. Liu, T. Liang, B. Zhang, L. Liu, Y. Zhao: *Materials Science and Engineering A*. 684, 2017, 261–269. <https://doi.org/10.1016/j.msea.2016.12.026>.

29. S. Huang, L. Li, Z. Peng, X. Xing, J. Gao, B. Wang: *Journal of Physics: Conference Series*, 2044, 2021. <https://doi.org/10.1088/1742-6596/2044/1/012098>.